CHAPTER-7

Structural, dielectric and electro-optic properties of a long chain biphenyl benzoate cored chiral mesogen and formulation of a room temperature ferroelectric liquid crystal mixture.

Part of this work has been published in Liquid crystal, Vol:43, pp1548-1549, 2016.

7.1 Introduction

The compound (*S*) - (+) -4′-[(3-pentadecafluorooctanoyloxy) prop-1-oxy]biphenyl-4-yl 4-(1-methylheptyl oxy)benzoate(7F3R) [1] has the highest number of fluorine atoms in its chain and is the longest member of the selected compounds. The molecular structure of the compound is shown in **figure 7.1**.

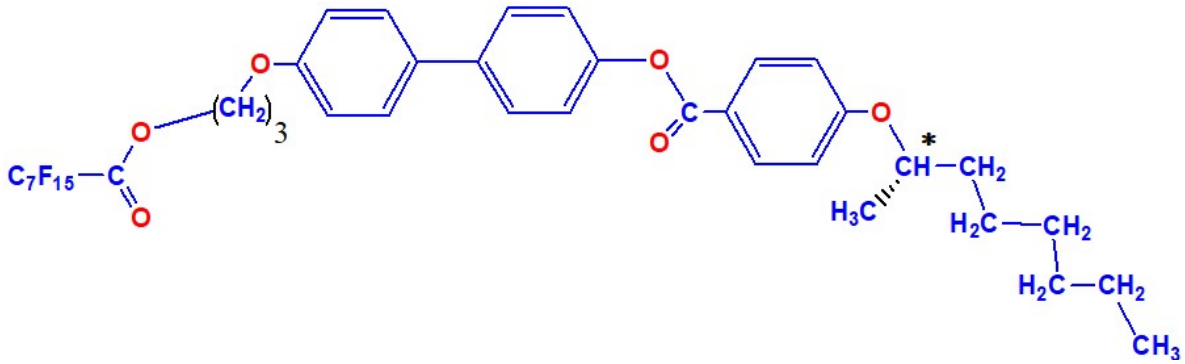

Figure 7.1: Molecular structure of 7F3R.

The compound has three oligomethylene spacers and seven carbons in its fluorinated chain. This compound exhibits largest range or highest stability of ferroelectric phase out of all the compounds included in this dissertation. It also gives rise to a paraelectric phase (SmA*) when heated beyond the ferroelectric phase, unlike the four compounds described in the last two chapters which melted directly to isotropic phase.

Main objective of studying the properties of different FLC systems is to find their comparative efficacy to FLC mixture formulation useful predominantly for display applications considering their microsecond order in-plane switching. It is well known that no single compound can satisfy all the properties required for such application like temperature range, switching time, optical birefringence, polarization, tilt angle, pitch, viscosity and above all thermal and UV stability [2–5]. Therefore, a mixture of achiral host molecules is normally doped with an appropriate

chiral molecule to formulate a useful FLC mixture. The host mixture is again usually a mixture of several achiral compounds with a reasonably wide range of SmC phase which controls the overall temperature range and tilt angle of the final mixture. Dopant is a compound with one or two chiral centres which controls the spontaneous polarization, viscosity, switching speed and helical pitch of the final mixture [6–10]. It might be noted that every component influences the properties of the resulting mixture, a particular property will depend not only on the type and proportion of chiral dopants, but also on the host materials used. However, the dopants are used to optimise the final properties to the desired level more effectively. Since 7F3R has the highest range of SmC* phase, therefore, we have chosen this compound to formulate a ferroelectric liquid crystal mixture.

In this chapter, we first present the structural, dielectric and electro-optic properties of the pure compound 7F3R. In the latter half we describe the formulation of the FLC mixture and results of the characterization of its properties.

7.2 Experimental procedure

For the Polarized optical microscopy (POM), small angle X-ray scattering (SAXS), dielectric and electro-optic studies, the material was fed into a polyimide coated planar dielectric glass cell of low resistivity and with transparent indium tin oxide electrodes of 8μm cell gap. The transition temperatures of the mixture were measured by differential scanning calorimeter (DSC), using a Mettler FP90 temperature controller, within an accuracy of ±0.1°C, along with FP84HT hot stage, in a heating cycle of rate 2°C/min. Phase transitions were also determined by investigating the optical textures of the compound by Olympus BX41

polarizing microscope equipped with a CCD camera using the same temperature controller.

Temperature dependent SAXS experiment was performed using PETRA III synchrotron beamline at P07 Physics Hutch station at Deutsches Elektronen- Synchrotron (DESY), Hamburg. An angular range (2θ) of ~ 5° was scanned using a beam of weave length 0.164 Å. Temperature in this experiment was controlled using a Lakeshore 340 temperature controller. For the mixture, SAXS experiment was done without applying any field as well as with field (12V/μm) across the cell. For the pure compound no field was applied.

Hioki 3532-50 impedance analyzer was used to measure the complex dielectric permittivity within the range 50Hz to 5MHz. The dielectric spectra were fitted using following modified Cole–Cole function[11]. Spontaneous polarization (P_S) was measured by time reversal method [12], using Agilent 33220A function generator by applying an triangular signal. Tektronix TDS 2012B digital storage oscilloscope was used to measure the voltage drop across a 100 kΩ resistance in series with the sample cell.

The details of all these experiments are discussed in chapter 2.

7.3 Characterisation of the pure compound

7.3.1 Observed phases

The phase sequence of the compound 7F3R was determined by combining the results of POM, SAXS and dielectric studies and is shown in **table 7.1**. Paraelectric SmA* phase is found to exist along with SmC* phase as mentioned before. It is worth noticing that SmA* phase was observed in the two short chain compounds of the series, namely, 1F3R

and 2F3R (discussed in chapter 3 and 4), but not in the intermediate derivatives studied in this dissertation. Thus this phase is found to reappear in the phase sequence with higher number of fluorine in its chain. Apart from that 7F3R shows the largest temperature span of SmC* phase (ΔT_{SmC*}): 72.5ºC out of all the compounds included in this dissertation.

Table 7.1. Transition temperatures and thermal stability of SmC^* phase of 7F3R

Compound	**Transition temperatures**	**stability of SmC^* phase (ΔT_{SmC*})**
7F3R	Crystal: 75.5 ^{0}C: SmC^* : 148.0 ^{0}C: SmA^* : 150.1 ^{0}C : Iso	72.5°

7.3.2 Polarized optical microscopy (POM) study

Optical textures of the compound in homogeneous geometry were recorded during cooling cycle. The textures of 7F3R at different phases are shown in **figure 7.2.**

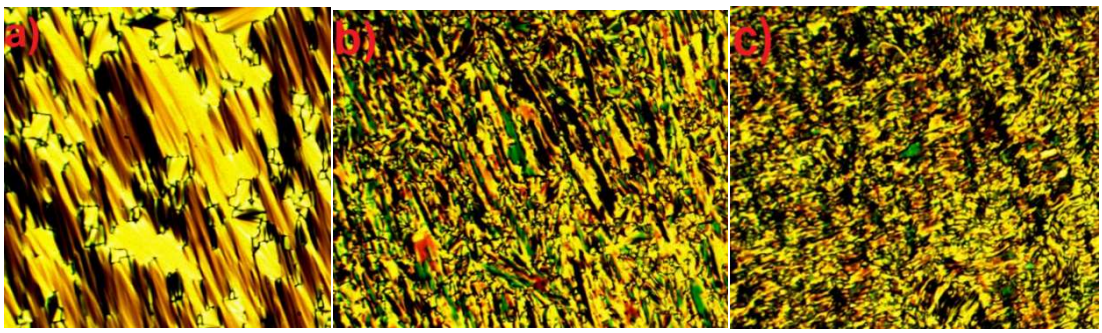

Figure 7.2: Optical texture of 7F3R at a) SmA* (149ºC) b) SmC* (114ºC) and c) crystal (74ºC) phases.

The signature fan shape texture [13] was observed in SmA* phase. After entering into SmC* phase the broken fan shape texture was observed with a little change in birefringence quite similar to what was observed in 2F3R (discussed in chapter 4). But unlike other compounds

the chiral lines were not distinctly visible even in SmC* phase. Absence of chiral lines are sometimes attributed to the smaller pitch of the compounds [13]. It can be mentioned here that for compounds with similar structures the pitch was reported to decrease with increasing number of fluorine atoms [1]. Since among the selected compounds, 7F3R has highest number of fluorine atoms so we can expect its pitch to be the lowest.

7.3.3 Optimised geometry

The molecular geometry of the compound was optimised applying Hartree-Fock method and using 3-21G basis set in a commercial package [14]. The optimised structure along with the direction of the dipole moment is shown in **figure 7.3**.

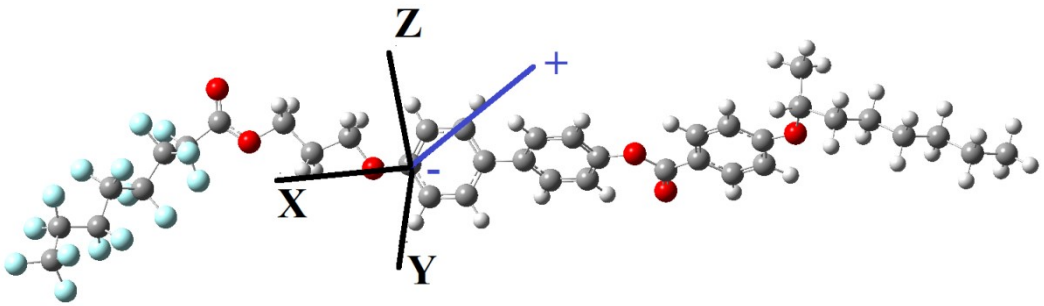

Figure 7.3: Optimised geometry of 7F3R.

The optimised length (*l*) of the compound is found to be 37.01Å, which is longer, as expected, than all the other compounds discussed in this dissertation. The dipole moment (μ) of 7F3R is found to be 6.55 D (-5.06, 0.4784, 4.14) where the components of dipole moments along the three coordinate axes are shown within parentheses as in other chapters. The dipole moment is found to be larger than all the other compounds since it is found to increase with increasing number of fluorines in the chain, except that of 1F3R and 2F3R, whose μ is still higher than 7F3R. This may be due to the twist of the fluorinated chain at the carboxylic group

by an angle ~85º which was observed in 3F3R and increased in all other higher derivatives including 7F3R. Thus 1F3R, 2F3R and 7F3R have larger dipole moments than the other compounds. This fact may have some relation with the presence of SmA* phase in these three compound and absence of the same in others.

7.3.4 Synchrotron diffraction study

Synchrotron diffraction studies were carried out in cooling cycle. In all the phases one sharp inner ring and one diffused outer ring were observed which correspond to smectic layer spacing and ordering within the layers respectively. Representative diffraction photographs of each phase are shown in **figure 7.4**.

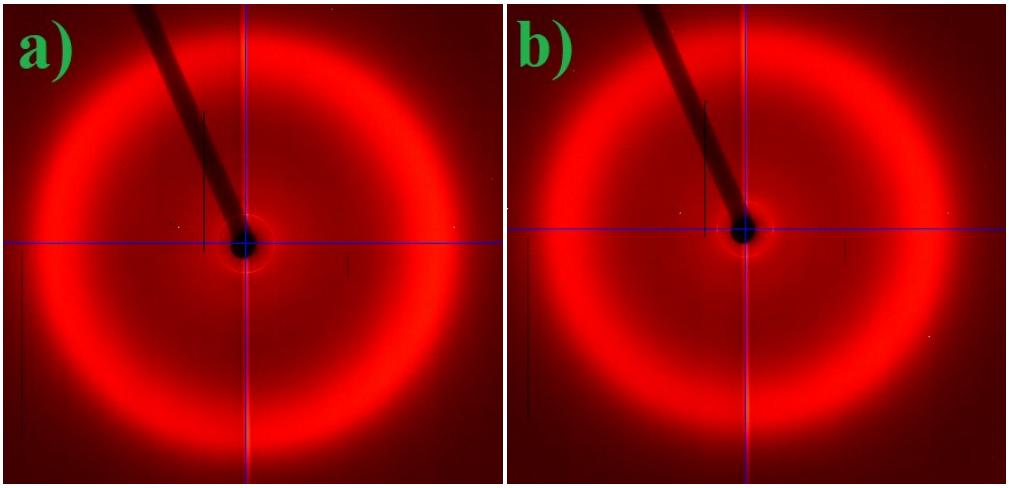

Figure 7.4: Diffraction photographs of 7F3R in a) SmC* (122ºC) and b) SmA* (149ºC) phases.

The layer spacings (d) were calculated from the low angle diffraction feature and the average intermolecular spacing (D) were calculated from the outer ring and these are depicted in **figure 7.5** as a function of temperature.

The layer spacing (d) is found to decrease with decreasing temperature in both the phases but a slight increase was observed near SmA*-SmC* transition. The layer spacing, however, is found to be less than the optimised molecular length (*l*) in both the phases, just like 2F3R as discussed in chapter 4.

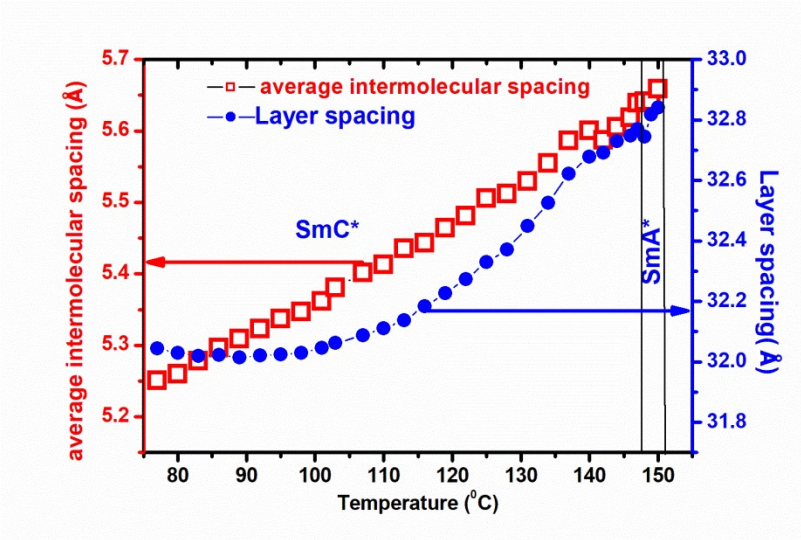

Figure 7.5: Temperature variation of layer spacing and average intermolecular spacing of 7F3R.

The ratio of layer spacing to molecular length (d/*l*) in SmA* phase was found to be nearly 0.88, which is less than 1F3R (1.07) and 2F3R (0.90). Thus d/*l* ratio is found to decrease with increasing chain fluorination. Moreover, this ratio was reported to be 0.50, 0.76, 0.97 for 5F6R, 4F6R and 1F4R respectively [1]. Hence it can be inferred that d/*l* ratio decreases even with increasing number of oligomethylene spacers. As the d/*l* ratio of 7F3R is less than one even in SmA* phase therefore SmA* phase may be de Vries type [15], as observed in 2F3R. To probe it further we have calculated the layer contraction in SmC* phase. The effective layer contraction was found to be 2.3% at 77ºC. Though this is higher

than that of 2F3R, but much less than ordinary SmA phase [16] and closer to de Vries type material [16,17].

In SmC* phase the temperature dependence of the layer spacing appeared to be parabolic. In accordance to the generalised mean field theory the tilt (θ) is $\theta \propto (T - T_C)^{\beta}$, where the value of the critical exponent β is expected to be (1/2) for a pure second order transition and (1/4) in case of second order transition approaching triclinic point. Following Hartley et al. [18] but keeping up to forth term in the expansion of cos(θ) it can be shown that near T_C

$$\frac{d_C}{d_A} \approx 1 - a|T - T_C|^{1/2} + b|T - T_C| \qquad [7.1]$$

when β is taken (1/4). Observed data fitted quite nicely to **equation 7.1**, signifying the SmC* to SmA* transition is probably tricritical type.

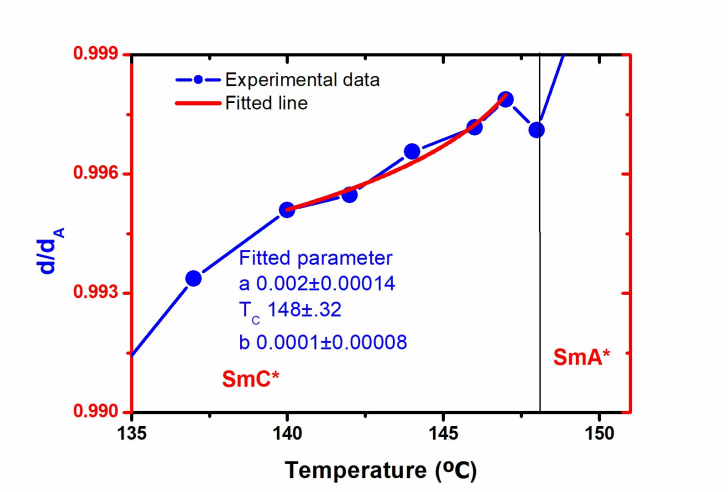

Figure 7.6: Temperature variation of d_C/d_A near transition.

The inter-molecular spacing is also found to increase with temperature as expected and it is (5.25 to 5.65 Å) of the same order as in 1F3R, 2F3R and 3F3R.

The molecular tilt angle was calculated from the relation, $= cos^{-1}\frac{d}{d_A}$, where d is the layer spacing at a particular temperature and d_A is the highest 'd' value at SmA phase. The temperature variation of the tilt angle is shown in **figure 7.7**.

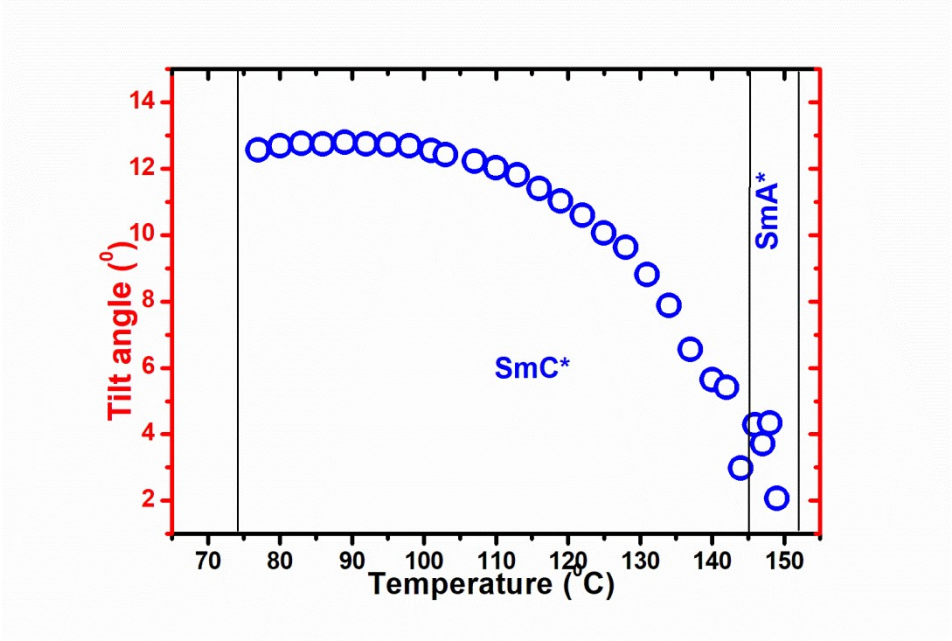

Figure 7.7: Temperature variation of X-ray tilt angle of 7F3R.

The tilt angle was much less than that of 2F3R (28.6º) and 3F3R (32.8º), but as discussed in chapter 2, in those cases the tilt was measured by dividing the layer spacing by the optimised molecular length to compare the values with other compounds having direct transition from SmC* to isotropic phase. However, as for the mixture we cannot have an exact value of the optimised length, so for the mixture and the dopant (7F3R) the tilt was calculated using the layer spacing in SmA* phase.

The correlation length (ξ) across and within the smectic layers was calculated using, $\xi = \frac{2\pi}{FWHM}$, where FWHM is the full width at half maxima in the scattering vector (Q) of the relevant Bragg's peak [19] and is shown in **figure 7.8**.

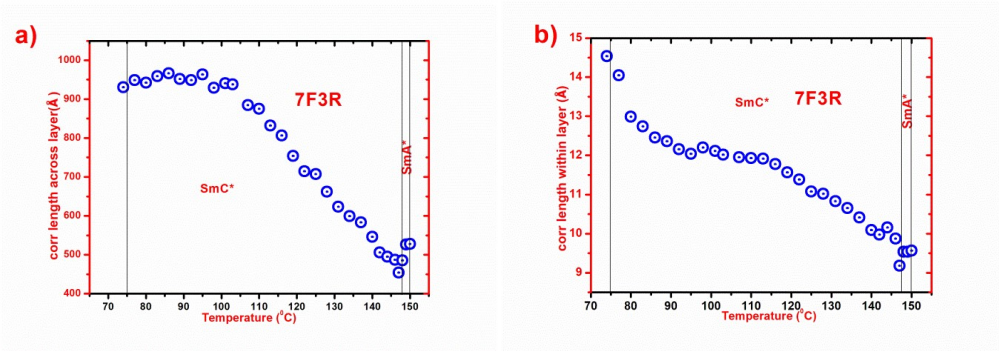

Figure 7.8: Correlation lengths of 7F3R a) across the layer and b) within layer.

The highest value of correlation length across and within layer in SmC* phase was found to be ~966Å and ~ 14Å respectively, which is slightly less than that of 2F3R and 3F3R. The correlation length across the layer was found to be approximately 26 times and 12 times of the optimised molecular length in SmC* and SmA* phases respectively. Surprisingly the correlation length across the plane, showed a little increasing trend after entering into SmA* phase.

7.3.5 Frequency dependent dielectric relaxation study

As discussed in chapter 2 the collective relaxation of SmC* phase is mainly dominated by Goldstone mode (GM) and soft mode (SM) relaxation. The Goldstone mode (GM) occurring at a lower frequency is associated with the azimuthal angle fluctuations of the directors in smectic planes and the soft mode (SM) is connected with the softening of the polar part of the tilt fluctuations which is seen throughout the SmA* phase and also in SmC* phase, but only near the transition temperature (T_C) [20]. Both these modes are observed. As a representative example, fitted dielectric spectra showing the presence of both the GM and SM in 7F3R is shown in **figure 7.9**. Fitted to Cole–Cole plot is shown in **figure**

7.10 Since the $\varepsilon^{/}$ and $\varepsilon^{//}$ are related to each other by Kramers- Kronig relation, Cole-Cole plot is to show that the fitting is good.

Goldstone mode relaxation is observed throughout the SmC* phase. This mode could be suppressed by applying proper DC bias. Near T_C another peak is seen at higher frequency range which sustained throughout the SmA* phase and did not vanish even under DC bias. This peak is associated with the soft mode relaxation. But as in 2F3R, here soft mode dielectric increment and critical frequency did not show respectively reverse 'V' shape and 'V' shape temperature variation in the vicinity of SmA*-SmC* transition as can be seen in **figure 7.11**. It is to be noted here, soft mode was observed before in 2F3R which also had both SmC* and SmA* phases, but not in other compounds which didn't have any orthogonal to tilted phase transition.

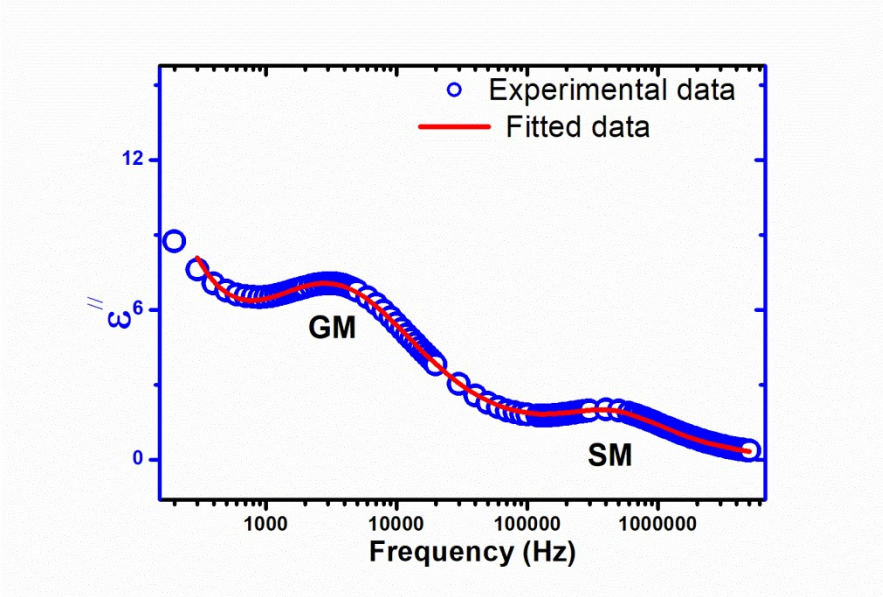

Figure 7.9: Fitted dielectric spectra in SmC* phase at 147.7ºC showing both GM and SM. Fitted parameters are $\Delta\varepsilon_{GM}$: 34.8±0.1, f_{CGM}: 3009 ±91.3, α_{GM}: 0.22± 0.003, $\Delta\varepsilon_{SM}$: 4.5±0.2, f_{CSM}: 365007±392, α_{SM}: 0.01± 0.003, σ :9.6E-8 ±1E-9.

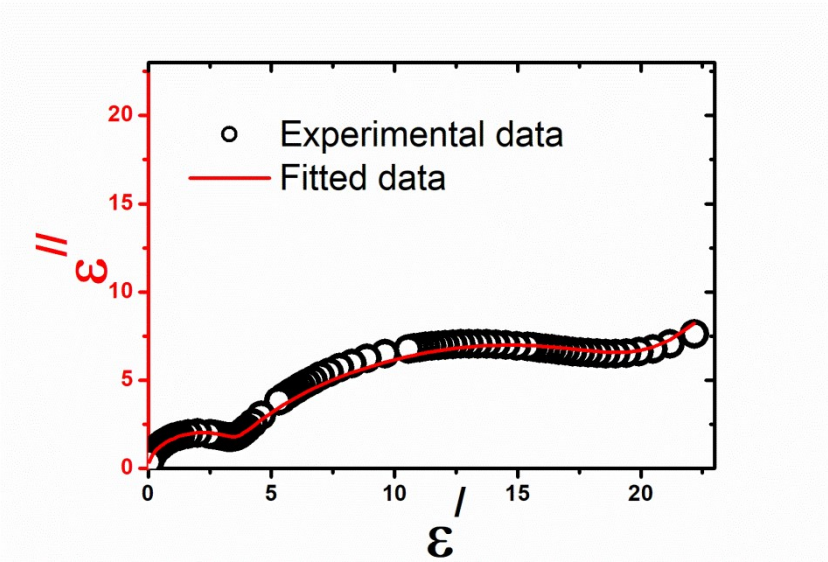

Figure 7.10: Fitted cole-cole plot at 147.7ºC

Relaxation frequency and dielectric increment observed from the fitted data are shown in **figures 7.11**, as functions of temperature.

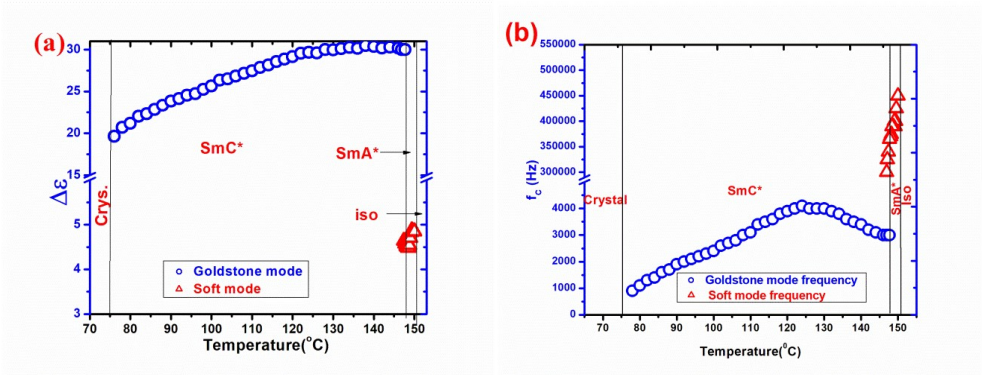

Figure 7.11: Temperature variation of a) dielectric increment and b) critical frequency of 7F3R.

The highest value of dielectric increment of Goldstone mode was found to be 30, much less than the other compounds discussed in this dissertation. GM critical frequency increased from 600 Hz (76°C) to 4100 Hz (124°C) and then decreased to 3000 Hz (146°C). Similar temperature variation was observed in 2F3R, 3F3R and 4F5R. However, the GM critical frequency of 7F3R was found to be much higher than all other compounds. For soft mode relaxation the critical frequency was

much higher than the GM critical frequency and it showed much stronger dependency with temperature as expected from generalized Landau model [21]. It increased from 300 kHz (147°C, SmC* phase) to 475 kHz (151°C, SmA* phase). The dielectric increment of soft mode was much smaller as noted, in comparison to its Goldstone mode counterpart which remained more or less constant with temperature.

7.3.6 Spontaneous polarization (P_S)

Temperature dependence of spontaneous polarization (P_S) is shown in **figure 7.12**.

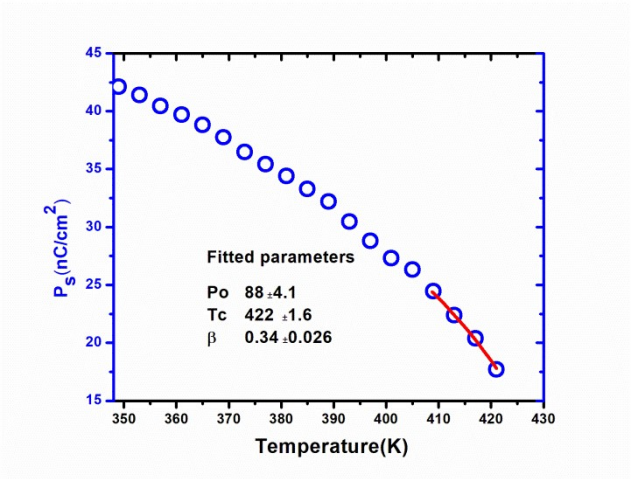

Figure 7.12: Temperature variation of spontaneous polarisation of 7F3R.

The spontaneous polarization (P_S) of the compound was found to increase with decreasing temperature as expected. The measured P_S data were fitted to the mean-field model, $P_S = P_0(1 - \frac{T}{T_C})^{\beta}$ [22] where T_C is the SmC* to SmA* transition temperature and β is critical exponent for the secondary order parameter P_S. β deviates significantly from the mean field value for a second order phase transition, however, fitted T_C matches nicely with observed T_C. It is worth mentioning that the change in enthalpy values at SmC* to SmA* transition was quoted as 1.61

kJ/mole in the reference [1]. This also indicates that the corresponding transition is not second order rather points to first order.

Maximum P_S value was found to be 42.1 nC/cm^2, which is higher than all other compounds with three oligomethylene spacers (2F3R, 3F3R, 5F3R and 6F3R). Thus P_S increases with fluorination for those compounds. However, P_S value of 7F3R is less than that of 4F4R and 4F5R. P_S strongly varies with the orientational order parameter (S) of the molecules, which depends on molecular length. It was reported previously that there is an optimal length of the molecule, for which P_S is maximum and any further increase in length results in decreased P_S [23]. Thus larger molecular length of 7F3R may cause its smaller P_S.

7.3.7 Rotational viscosity (γ_φ) and Response time (τ)

The temperature variation of rotational viscosity and response time is shown in **figure 7.13**.

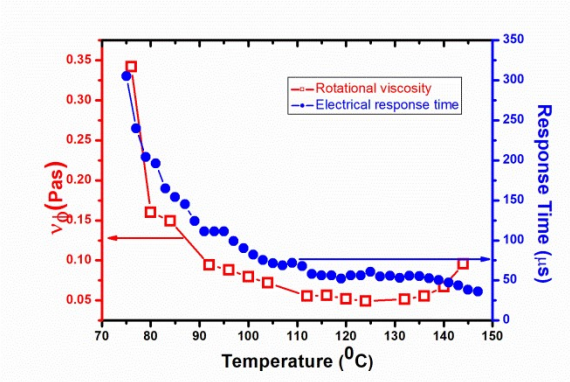

Figure 7.13: Temperature variation of rotational viscosity and response time.

The rotational viscosity in Goldstone mode was determined using the following relation $\gamma_\varphi = \frac{1}{4\pi\varepsilon_0}\frac{1}{\Delta\varepsilon f_C}(\frac{P_S}{\theta})^2$ derived from generalized Landau model [21], where Goldstone mode dielectric strength ($\Delta\varepsilon$) and relaxation frequency (f_C) were obtained from dielectric relaxation study and tilt

angle (θ) was obtained from electro optic measurement (described in section **7.3.8**). Highest value of rotational viscosity was found to be 0.34 Pas. Rotational viscosity first decreases with temperature, then near the SmC* to SmA* transition it diverges which may be due to pre-transitional effect.

The highest value of response time was found to be ~ 300 μs which is larger than all other nF3R compounds. However, it decreased rapidly with temperature and near SmC*-SmA* transition reduced to below 50 μs.

7.3.8 Optical tilt angle

Tilt angles for the compound was also determined optically and have been depicted in **figure 7.14**.

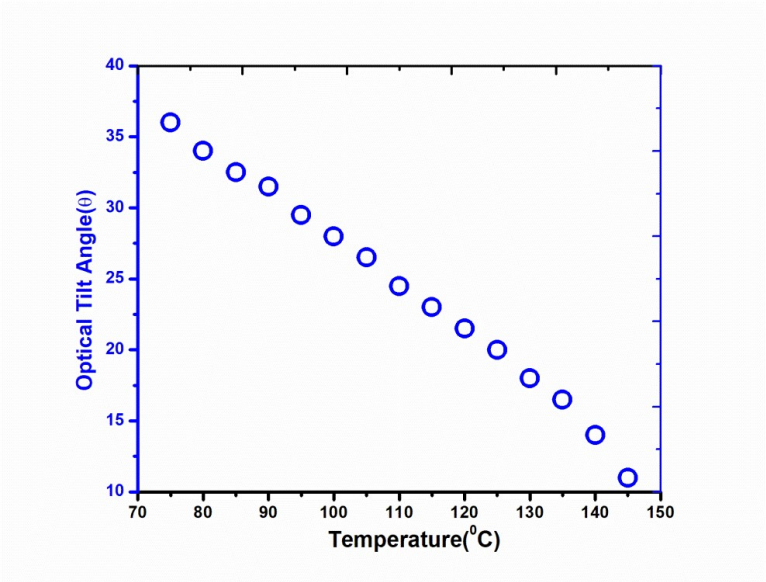

Figure 7.14: Temperature variation of optical tilt angle.

Optical tilt reflects the angle between the direction of molecular core and the layer normal. The highest value of optical tilt was found to be ~36º which is higher than all other compounds whose tilt has been

measured optically in this dissertation. The X-ray tilt, shown in **figure 7.7**, was observed to be much less than optical tilt. X-ray tilt arises from the tilt of electron-density function of the whole molecule, on the other hand optical tilt is a result of tilt of only the rigid polarisable group of the molecule, thus the two tilts may differ. This difference depends on the zig-zag shape of the molecules[24]. The zig-zag molecular shape coming out of the rigid core may tilt independently whereas the melted end chains are on the average closer to the layer normal. The X-ray tilt was observed to be less than optical tilt when the chain of a zig-zag molecule are in trans position [1].

7.4 Formulation and characterisation of a room temperature ferroelectric liquid crystal mixture using 7F3R as dopant

7.4.1 Formulation of the mixture

As discussed in the introduction section, ferroelectric liquid crystals (FLC) can be promising in display application for their high speed switching. However most of the FLCs exhibit ferroelectric behaviour at higher temperatures, a fact also observed in all the compounds studied in this dissertation. Thus there has been constant effort to formulate multi-component ferroelectric liquid crystal mixtures, which would show ferroelectric phase even at and below room temperature. We have successfully formulated a FLC mixture, which showed ferroelectric SmC* phase at room temperature and beyond, by doping 7F3R into an achiral host mixture (HM) having smectic C phase. The host matrix was formulated by mixing four pyrimidine based achiral compounds (H1, H2, H3 and H4). The molecular structures and phase sequences with

transition temperatures of these compounds and that of the host matrix are shown in **table 7.2**. The mixture was formulated following similar procedure reported previously by our group [25].

To prepare the mixtures, weights of the individual pure compounds were measured by a weighing balance (Sartorius-CPA225D, Germany) having accuracy of ±0.01mg and then were mixed (in various wt% as required) in a cleaned glass bottle. Chloroform was added to make the mixtures homogeneous and was ultrasonicated (GT Sonic Professional, Apex, India) at 65°C for four hours to evaporate chloroform completely. The complete evaporation of chloroform was confirmed by regaining the weight of the mixture. The FLC mixture was produced by mixing 30 wt% of 7F3R with 70 wt% of HM.

7.4.2 Observed phases of the mixture

Initially we mixed 10 wt% and 20 wt% of 7F3R in the host matrix, but in these mixtures no polarity was induced. But when 30 wt% of 7F3R was mixed in the host matrix, polarity could be induced and the ferroelectric SmC* phase continued far below room temperature, to around 15°C beyond which we couldn't investigate. It is relevant to note here that 4F3R was also found to induce polarity only at a minimum of 40 wt% [26], thus 7F3R induced polarity at lower concentration. Moreover, it was found to retain the SmA* phase of the dopant albeit over a larger temperature range. The phase sequence and transition temperatures of the mixture are given in **table 7.3**. The range of the SmC* phase (ΔT_{SmC*}) was found to be at least 59°, which is moderately high but less than that of the dopant (72°). However, unlike the dopant, the mixture exhibits SmC* phase even below room temperature whereas the dopant formed SmC* phase at as high as 75.5°C.

Table 7.2 Molecular structure and transition temperatures of host molecules and host mixture

H1	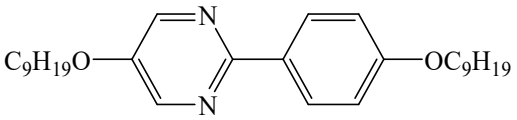
	Cr 61.8ºC SmC 95.6ºC SmA 99.1ºC I
H2	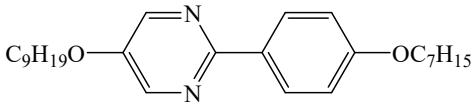
	Cr 57.4ºC SmC 95.1ºC SmA 98.4ºC I
H3	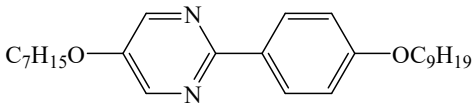
	Cr 57.2ºC SmC 79.1ºC SmA 91.2ºC N 94.7ºC I
H4	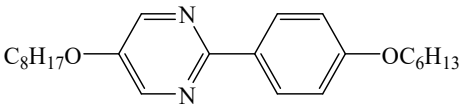
	Cr 27.5ºC SmC 46.3ºC SmA 57.5ºC N 65.6ºC I
HM	H1 20wt% + H2 20wt% + H3 20wt% + H4 40wt%
	Cr 19ºC SmC 69.4ºC SmA 78.7ºC N 81.2ºC I

Table 7.3: Phase sequence and transition temperature of the mixture

Composition:	HM (70 wt%) + 7F3R (30 wt%)
	~15°C < SmC* 74.3°C SmA* 101.4°C Isotropic

7.4.3 Polarised optical microscopy (POM) and Differential Scanning Calorimetry (DSC) study

The transition temperatures and the phase behaviour of the mixture were investigated both by POM and DSC studies. The transition temperatures matched more or less in both the processes. The DSC theromogram, showing the variation of heat flow with temperature in a cooling cycle is shown in **figure 7.15**. Peaks in the thermogram were observed at temperatures 74.3°C and at 101.4°C. It is noted that the clearing point peak is much flatter than the other one. Clearing started from a temperature ~ 96°C and continued till ~ 105°C which indicates that the transition from SmA* to the isotropic phase is not a sharp one.

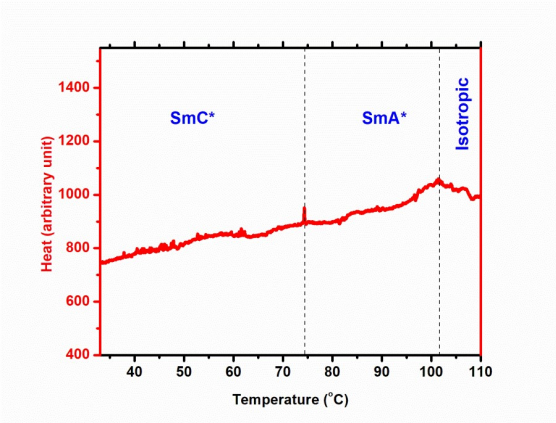

Figure 7.15: DSC thermogram of the mixture during cooling.

Observed textures are shown in **figure 7.16**. Within the temperature range 74-101°C the mixture showed clear fan shaped texture, typically observed in SmA* phase [13]. Below 74°C the texture changed to broken fan shape. A change in birefringence was also noticed. However, no chiral lines were observed, as is usually seen in SmC* phase. As noted before, even in the optical texture of pure 7F3R the chiral lines were not visible and this might be due to short pitch. Change in colour may be due to change in tilt and birefringence with temperature[13]. From about 90°C, domains of isotropic phase could be observed within the SmA* texture. This seems to be in conformity with the DSC observation that asserted a continuous transition to isotropic phase rather than a sharp one.

Although no chiral lines could be observed in SmC* phase, switching of the molecules was observed under an ac field of strength 0.12 V/µm which confirmed the ferroelectric nature of the phase. Switching could also be observed at 2.0 V/µm field in SmA* indicating the presence of electroclinic effect.

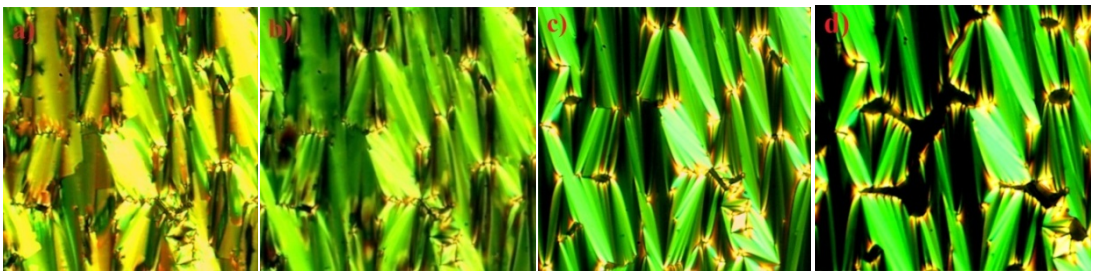

Figure 7.16: Textures of the mixture at temperature a) 33°C (SmC*) b) 63°C (SmC* with changed birefringence) c) 85°C (SmA*) and d) 93°C (SmA* with isotropic domain).

7.4.4 Synchrotron diffraction study

Synchrotron diffraction studies were carried out on the mixture and also on the constituent compounds to compare their structural properties.

In all the phases one sharp inner ring and one diffused outer ring were observed. Representative diffraction photographs of the host compound in SmC phase and of the mixture in SmC* and SmA* phase are shown in **figure 7.17** and **7.18** and intensity profiles of inner and outer maximum of the mixture are shown in **figures 7.19** and **7.20.** The layer spacing (d), average intermolecular spacing (D) and X-ray tilt angle were calculated by the same procedure described before.

To inculcate the structural properties, temperature variation of layer spacing and X-ray tilt of the host matrix (HM) are plotted along with those of the host matrix components (H1,H2, H3 and H4) and are shown in **figure 7.21**.

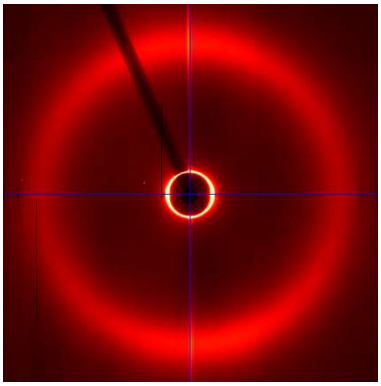

Figure7.17: Diffraction photograph of HM in SmC phase (60ºC)

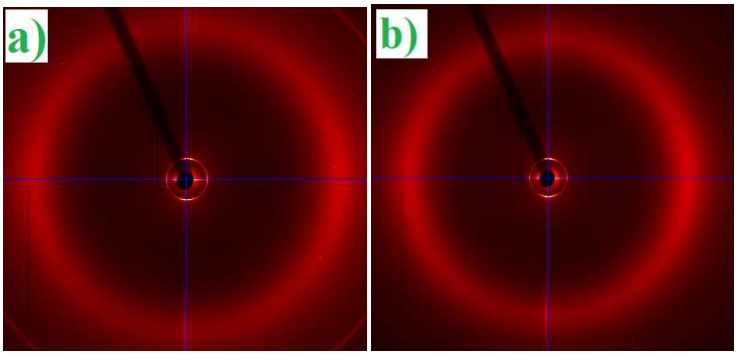

Figure 7.18: Diffraction photograph of the mixture in a) SmC* (66ºC) and b) SmA* (84ºC) phases.

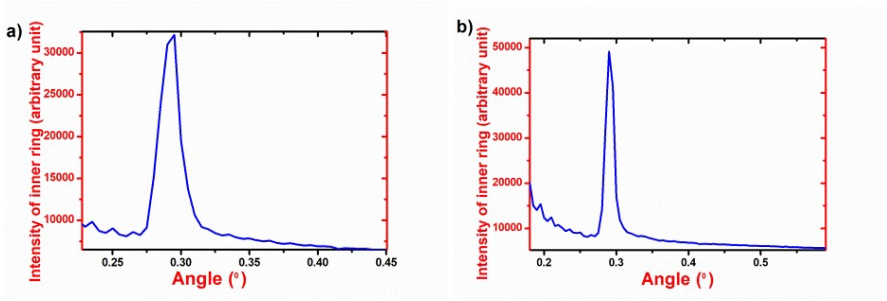

Figure 7.19: The intensity profile of the inner maxima of X- ray photograph in a) SmC* (66ºC) and b) SmA* (84ºC) phases of the mixture.

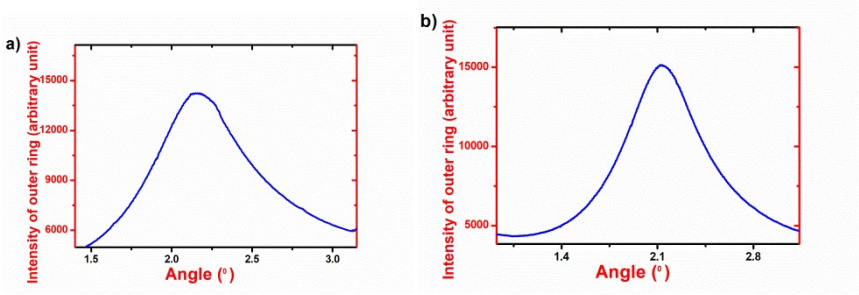

Figure 7.20: The intensity profile of the outer maxima of X- ray photograph in a) SmC* (66ºC) and b) SmA* (84ºC) phases of the mixture.

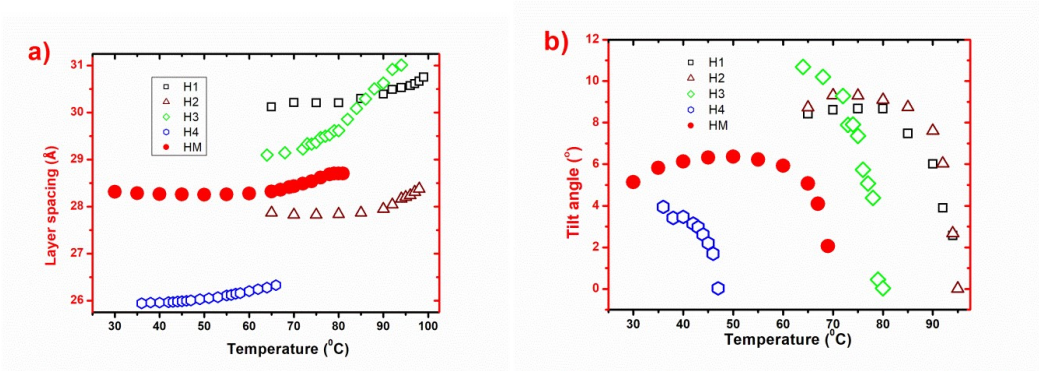

Figure 7.21: Temperature variation of a) layer spacing and b) tilt angle of H1, H2, H3, H4 and HM.

For all the compounds the layer spacing increased and tilt angle decreased with temperature as expected. The rate of increase of 'd' with temperature was found to be highest for the constituent H3. In HM layer spacing was found to have a marginal increasing trend with temperature even within SmA phase and became constant after entering into the nematic phase. Layer spacing of the host matrix is found to be almost equal to the weighted average layer spacing of the constituents, but the tilt is lower. The minimum and maximum 'd' values of the mixture diverged only by 0.52 Å and 0.2Å from the respective weighted average 'd' values of the constituents. But for tilt these differences are higher, respectively being 1.5° and 1.6º.

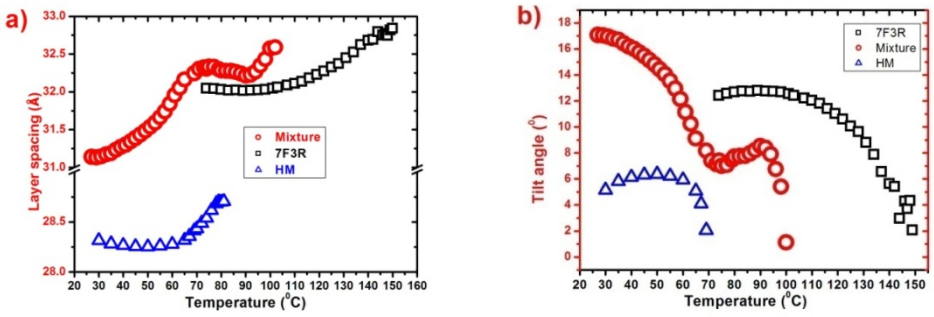

Figure 7.22: Temperature variation of a) layer spacing and b) tilt angle of the mixture, HM and 7F3R.

Temperature evolutions of layer spacing and tilt angle compared to the host matrix and the dopant have been presented in **figure 7.22**. In the low temperature region of SmC* phase the layer spacing of the mixture is in between the host and the dopant (if we extrapolate the values of dopant to low temperature). However, the maximum value of the layer spacing of the mixture in SmC* phase (32.3 Å) is found to be closer to that of the dopant (32.8Å) rather than in the host matrix (28.7Å). On the other hand, in the low temperature region of SmC* phase the tilt is much higher in the mixture than in the host and the dopant. The maximum tilt of the

mixture in SmC* phase is found to be moderate (~17°) and it decreased with temperature as expected. Thus the mixture had more suitable tilt than the dopant 7F3R, to use in SSFLD, where ideally a tilt of 22.5° is preferred [27].

To analyse further the temperature evolution of layer spacing in the mixture in different phase it has been shown separately in **figure 7.23**. It is noted here that temperature scan could be carried out till only 27°C in the diffraction experiment.

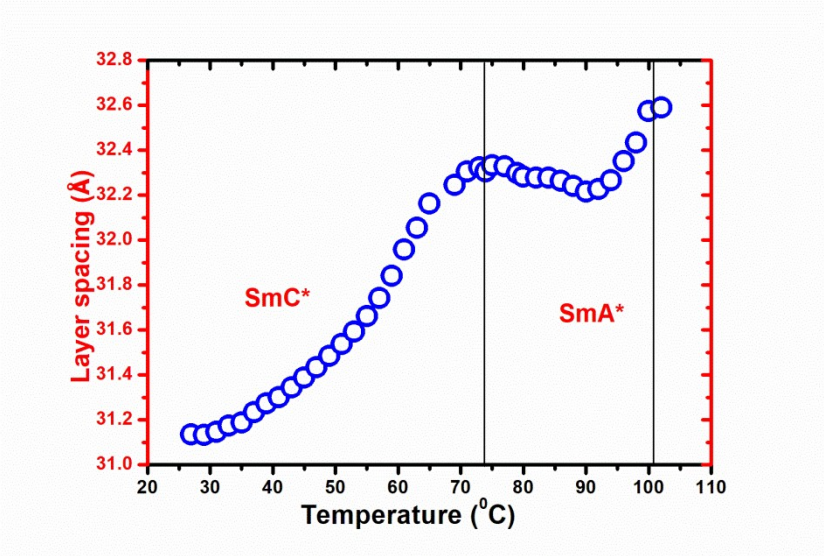

Figure 7.23: Temperature variation of layer spacing of the mixture.

The minimum value of layer spacing in SmC* phase was found to be 31.13Å which increased with temperature as expected. But in SmA* phase 'd' value first decreased and then increased with temperature. However, its maximum value (~32.6Å) was found to be less than the weighted average of the optimised molecular lengths of the constituent molecules (32.75Å), just like in the dopant 7F3R. It indicates that the mixture may exhibit de vries type SmA* phase. The increasing trend of 'd' with temperature within SmA* phase from a temperature ~92°C may be due to pre-transition effect. It can be recalled that from DSC and POM

data it was inferred that isotropic domains seem to form within SmA* phase from that temperature range. Below that temperature d value showed a negative thermal expansivity which is seen in a de veries like SmA* phase [16,28]. The highest layer shrinkage in SmC* phase was found to be only 3% which is still much less than normal SmA* phases [29,30]. However, the layer shrinkage is more than that of pure 7F3R (2.3%). To probe this further we have calculated, using **equations 7.2** and **7.3**, the figures of merits 'R' and 'f' defined by Radcliffe *et al.* [16,31] to gauge the capability of a de veries type material to achieve defect free book shelf geometry.

$$R = cos^{-1}\left[\frac{d_c(T)}{d(T_{AC})}\right]/\theta_{OPT}(T) \qquad [7.2]$$

$$f = cos^{-1}\left[\frac{d_c(T)}{d_A(T)}\right]/\theta_{OPT}(T) \qquad [7.3]$$

Here, $d_C(T)$ is smectic layer spacing at T, d (T_{AC}) is layer spacing at SmC* to SmA* transition, $d_A(T)$ is the layer contraction relative to SmA* layer spacing extrapolated to SmC* phase, and $\theta_{OPT}(T)$ is the optical tile angle (optical tilt of the mixture will be reported in section **7.4.5**).

R and f are found to be 0.34 and 0.36 respectively in 7F3R which are in excellent agreement with the de Veries like compounds capable of having defect free bookshelf geometry [16,32]. However, in the mixture these values are found to be 0.71 and 0.79. Though 'de veries like character' has been compromised to some extent in the mixture, but comparing the 'R' and 'f' values (~0.8) of other reported partially de veries like compounds [32,33], it can be concluded that there is partial de veries like characteristics even in the mixture.

To see the effect of electric filed on the mixture property, tilt angles had been measured both without and with application of a dc field of 12V/µm across the measuring cell. These results are shown in **figure 7.24**. In the mixture in SmA* phase a tilt of ~8° was observed even without external field, which might be related with its de Vries like character. After application of field, tilt angle increased in both phases and electroclinic effect was observed in SmA* phase where the tilt increased by ~ 2.5°.

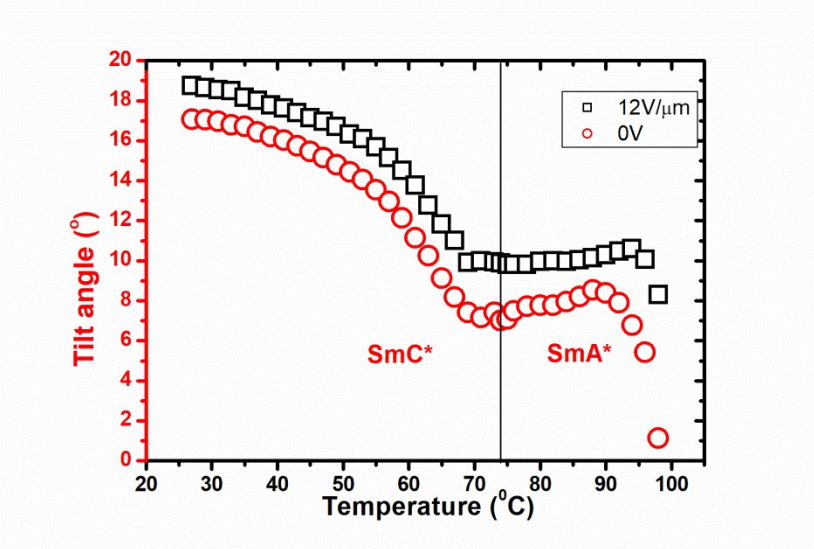

Figure 7.24: Temperature variation of X-ray tilt of mixture with and without bias.

To explore the positional correlation of the molecules in different phases of the mixture, the correlation lengths across and within the layers were measured from the full width at half maxima of the scattering vector of corresponding Bragg's peak. The temperature variations of the correlation lengths in the mixture are shown in **figure 7.25**, variations in the dopant are also shown for ease of comparison.

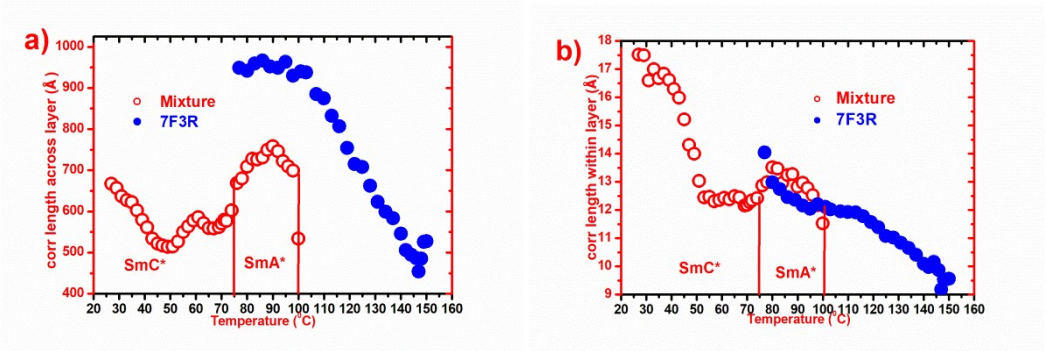

Figure 7.25: Correlation lengths of the mixture and the dopant a) across the layers and b) within the layers.

It is observed that the correlation length across the layer ($\xi_{\parallel}$) in the mixture decrease slightly from that of dopant 7F3R. In 7F3R it is found to be about 26 times of its molecular length, while in the mixture it is about 23 times of the weighted average of the molecular lengths of the constituent compounds. Surprisingly this correlation length is found to increase by ~ 100Å in SmA* phase than in SmC* phase following the same trend as was observed even in 7F3R. The correlation length of the mixture within the layers ($\xi_{\perp}$) is found to be maximum in SmC* (17.5Å), then it decreases with temperature. However after entering into SmA* phase it increased marginally. In the common temperature range correlation lengths ($\xi_{\perp}$) of the dopant and the mixture are found to be comparable for 7F3R and the mixture, with a minor increase in the mixture. No appreciable change in correlation lengths were observed under the influence of electric field.

7.4.5 Spontaneous and induced polarization (P_S)

The temperature variation of P_S of the mixture is shown in **figure 7.26**. The P_S was measured with a voltage 19V/μm which was the saturation field (discussed below). In SmC* phase the spontaneous polarization

initially increased with temperature and reached its highest value (31.7 nC/cm^2) at 46ºC and then was found to decreased with temperature as expected. The highest value of spontaneous polarization in SmC* phase (31.7 nC/cm^2) was found to be less than that of 7F3R (42.1 nC/cm^2) (discussed in section **7.3.6**). In electroclinic SmA* phase the total polarization (P_S) consists of two parts: one part represents the orientation and electronic polarization and the second part is due to P-θ coupling [34]. It is difficult to separate these two parts, so, in SmA* phase by P_S we represent the total induced polarization. Moderate value of P_S (24.6 nC/cm^2) was observed in the electroclinic SmA* phase. Such moderate values of induced polarization in electroclinic SmA* phase were reported previously in other chiral compounds [35,36] as well. P_S changed almost continuously at SmC* to SmA* transition. In de Vries type SmA* phase such continuous change in Ps was reported before and this is expected as in addition to usual electroclinic effect, here the induced polarization is also a result of "the biasing of the molecular azimuthal distribution perpendicular to the electric field"[35].

Near the SmA* to isotropic transition the measured data was fitted to the mean field model $P_S = P_0(1 - \frac{T}{T_C})^{\beta}$, [24] where T_C is the SmA* to isotropic phase transition temperature and β is the critical exponent of second order parameter. T_C is not found to deviate more than 1°C from the observed data in the mixture. β is also found to be 0.21which is comparable to the value (0.25) predicted by Landau theory at the cross over (triclinic) point from 2nd order to 1st order transition [33,37].

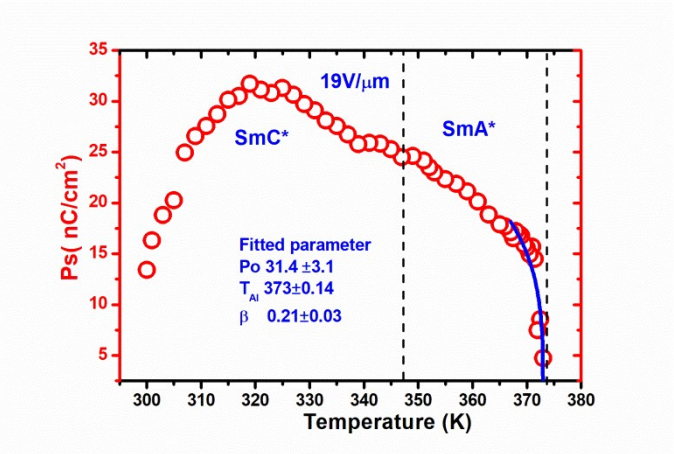

Figure 7.26: Temperature variation of P_S of the mixture.

To explore the bias dependence of P_S, spontaneous polarization was measured as a function of voltage at two particular temperatures in two different phases as shown in **figure 7.27**. In SmC* phase switching was observed at a minimum field of 0.12V/μm, however, in SmA* phase about twenty times more field was required (2V/μm) to observe the switching. But due to noise in signal at low voltage, P_S could be reported only at a minimum voltage of 4V/μm. In both phases P_S was found to increase with applied voltage and ultimately reached saturated polarization at a field of ~19 V/μm. P_S was also measured with decreasing voltage to see the hysteresis effect. In SmC* phase appreciable hysteresis was observed, which might be useful in terms of memory effects in FLC [38]. In SmA* phase also hysteresis could be observed, but the effect is less than that in SmC* phase.

Similar increase of induced polarization with applied electric field in electroclinic de Vries type SmA* phase was reported before [35]. For de Vries like SmA* phase, this variation can be explained if we consider the reorientation of the molecular dipoles in presence of electric field is of Langevin type and assume that the effective dipole moment (μ_{eff}) will also increase with the applied field [35]. μ_{eff} can be calculated from the

relation $\mu_{eff} = \pi d(\frac{\xi_\perp}{2})^2 P_s$ derived from Langevin formula [35], where $\xi_\perp$ is the correlation length within a layer, d is the layer spacing and P_S is induced polarization. The effective dipole moment has been calculated for the mixture in SmA* phase (77ºC) as a function of applied voltage and is shown in **figure 7.28**.

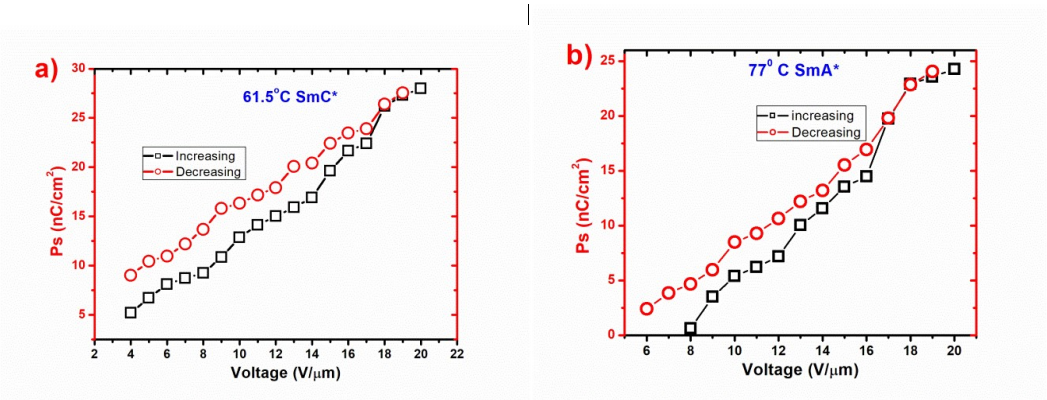

Figure 7.27: Field variation of P_S in a) SmC* and b) SmA* phases.

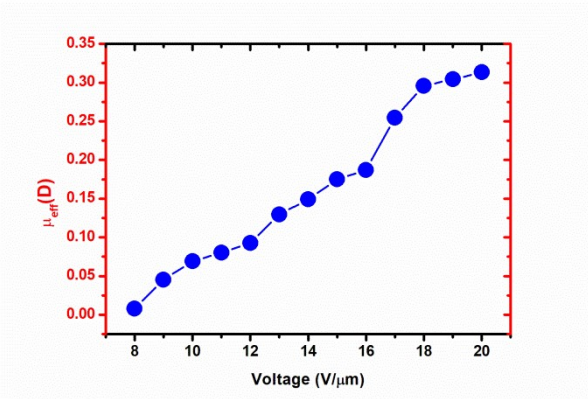

Figure 7.28: Dependence of effective dipole moment on applied field in SmA* phase (77ºC).

μ_{eff} increases with applied voltage as expected and reached a saturation value of ~ 0.32 D near 19V/μm. The saturated value of the dipole moment is comparable with the perpendicular component of molecular dipole moment of 7F3R (0.47D), obtained by optimising the molecular structure as discussed in section 7.3.3.

7.4.5 Optical tilt angle (θ)

The optical tilt angle of the mixture was measured in both SmC* and SmA* phases with an applied voltage of 16V/µm as shown in **figure 7.29**. The θ was found to decrease with temperature as expected. Highest tilt in SmC* phase was 20.6°. Even in SmA* phase it was as high as 17°, which established the electroclinic behaviour of the compound once again. For the ease of comparison the X-ray and optical tilt of the mixture and 7F3R are shown together in **figure 7.30**. The optical tilt of the mixture was found to be much less compared to the dopant 7F3R but it was found to be comparable but marginally higher than X-ray tilt. In the mixture tilt angle was also measured at a particular temperature in SmA* phase as a function of applied voltage and is shown in **figure 7.30**. This clearly shows that induced tilt is linear function of applied field at low field region and at higher field it saturates.

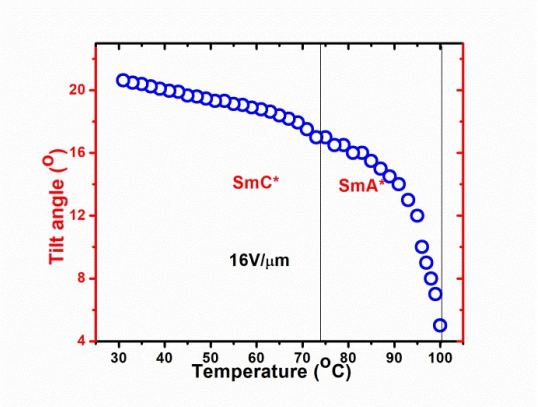

Figure 7.29: Temperature variation of optical tilt of the mixture.

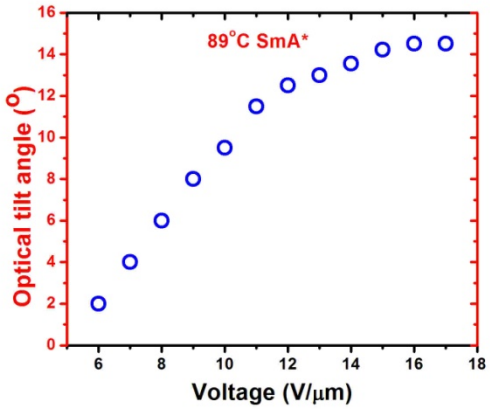

Figure 7.30: Bias dependence of optical tilt of the mixture at temperature 89°C (SmA*).

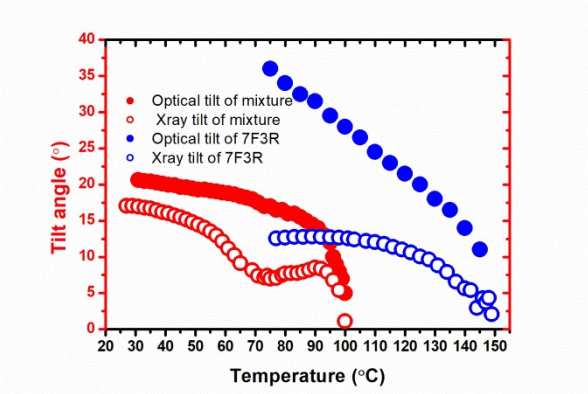

Figure 7.31: The X-ray and optical tilt of mixture and 7F3R.

7.4.6 Response time (τ)

Response time is one of the most important parameter from application perspective. In pure 7F3R the highest rise time in SmC* phase was found to be 300μs. In the mixture the response time decreased significantly probably because of lower viscosity which makes the mixture more suitable for fast display applications. Temperature dependence of τ, measured at a voltage 11V/μm for the mixture is shown in **figure 7.32**. In SmC* phase τ was found to be ~ 215 μs. In SmA* phase it decreased

again. The maximum value of response time in SmA* phase was found to be ~190μs. Though this value is higher than in many electroclinic compounds [36], but response time in order of few hundred microsecond had also been reported before for electroclinic de Vries type compounds [35,39].

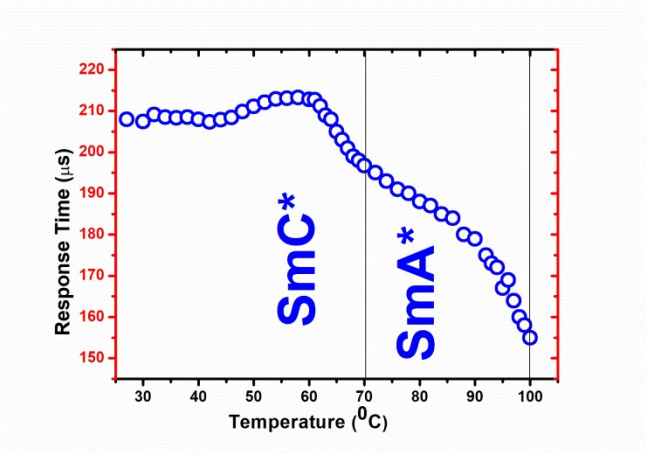

Figure 7.32: Temperature variation of rise time of the mixture.

7.5 Conclusion

The compound 7F3R, having highest number of fluorine atoms in the chain, exhibits SmC* phase for the widest span of temperature among the selected compounds. The compound is also found to have de Vries type SmA* phase. It showed both GM and SM relaxation modes. It showed high optical tilt and sharp electrical response time. An FLC mixture is obtained by doping 30% 7F3R in an achiral pyrimidine based host mixture, for the lower homologue 4R3R minimum 40% doping was necessary for inducing polarity. While the dopant produce ferroelectric phase from 75.5^{o}C, the mixture is found to exhibit ferroelectric SmC* phase from below room temperature and the phase is found to exist over a wide temperature range. It also shows SmA* phase before melting into isotropic phase. Further, the SmA* phase is found to exhibit partial de

Vries type property and electroclinic effect. In the low temperature region of SmC* phase the layer spacing of the mixture is in between the host and the dopant while the tilt is found to be much higher in the mixture than in the host and the dopant. It was found to have moderate spontaneous polarization. Optical tilt of around 20° at room temperature and a response time of a few hundred microseconds make the mixture suitable to use in SSFLCDs. It is expected that problem of chevron defect and hence reduced contrast ratio will be minimum since highest layer shrinkage of in SmC* phase is 3%. Further, the mixture in SmC* phase shows appreciable hysteresis which might be useful in terms of memory effects in FLC.

Reference

[1] Ziobro D, Dąbrowski R, Tykarska M, et al. Synthesis and properties of new ferroelectric and antiferroelectric liquid crystals with a biphenylyl benzoate rigid core. Liq. Cryst. 2012;39:1011–1032.

[2] Maltese P. Advances and problems in the development of ferroelectric liquid crystal displays. Mol. Cryst. Liq. Cryst. Sci. 1992;215:57–72.

[3] Rudquist P. Orthoconic antiferroelectric liquid crystals. Liq. Cryst. 2013;40:1678–1697.

[4] Takezoe H, Gorecka E, Čepič M. Antiferroelectric liquid crystals: Interplay of simplicity and complexity. Rev. Mod. Phys. 2010;82:897–937.

[5] Hird M. Ferroelectricity in Liquid Crystals and Its Applications. Liq. Cryst. 2011;38:1467–1493.

[6] Bennis N, Dąbrowski R, Spadlo A, et al. Non-conventional alignment surfaces for antiferroelectric liquid crystals. Mol. Cryst. Liq. Cryst. 2004;422:307–316.

[7] Kuczyński W, Stegemeyer H. Ferroelectric properties of smectic C liquid crystals with induced helical structure. Chem. Phys. Lett. 1980;70:123–126.

[8] Thurmes WN, Wand MD, Vohra RT, et al. FLC materials for microdisplay applications. Proc. Spie. 1997;3015:1–6.

[9] Wand MD, Vobra R, Thurmes W, et al. NEW FERROELECTRIC LIQUID CRYSTAL HOST MATERIALS FOR USE IN

OPTOELECTRONIC APPLICATIONS. Proc. Spie. 1994;2175:2–7.

[10] Wand M, Thurmes W, Meadows M, et al. FLC Displays for High Resolution Magnified View and Projection Applications. Proc. Spie. 1999;3635:2–7.

[11] Böttcher C, Belle O, Rip A, et al. Theory of Electric Polarization, Vol II. Amsterdam, New York: Elsevier, Scientific Publishing Co; 1973.

[12] Miyasato K, Abe S, Takezoe H, et al. Direct Method with Triangular Waves for Measuring Spontaneous Polarization in Ferroelectric Liquid Crystals. Jpn. J. Appl. Phys. 1983;22:L661–L663.

[13] Dierking I. Textures of Liquid Crystals. wiley-vch. Weinheim: WILEY-VCH; 2003.

[14] Gaussian 09, Revision D.01, M. J. Frisch *et al.* Gaussian, Inc., Wallingford CT, 2013.

[15] Agra-Kooijman DM, Yoon H, Dey S, et al. Origin of weak layer contraction in de Vries smectic liquid crystals. Phys. Rev. E 2014;89:032506.

[16] Singh HK, Singh SK, Nandi R, et al. Observation of exceptional 'de Vries-like' properties in a conventional aroylhydrazone based liquid crystal. RSC Adv. 2016;6:57799–57802.

[17] Sreenilayam SP, Rodriguez-Lojo D, Agra-Kooijiman D, et al. De Vries liquid crystals based on a chiral 5-phenylpyrimidine benzoate core with a tri- and tetra-carbosilane backbone tetra-carbosilane

backbone. Phys. Rev. Mater. 2018;2:025603-1-025603–025612.

[18] Hartley CS, Kapernaum N, Roberts JC, et al. Electroclinic effect in chiral SmA* liquid crystals induced by atropisomeric biphenyl dopants: Amplification of the electroclinic coefficient using achiral additives. J. Mater. Chem. 2006;16:2329–2337.

[19] Sirota EB, Pershan PS, Sorensen LB, et al. X-Ray Studies of Tilted Hexatic Phases in Thin Liquid-Crystal Films. Phys. Rev. Lett. 1985;55:2039–2042.

[20] Hasse W, Wróbel S. Relaxation Phenomena: Liquid Crystals, Magnetic Systems, Polymers, High-Tc Superconductors, Metallic Glasses. Berlin: Springer; 2003.

[21] Carlsson T, Žekš B, Filipič C, et al. Theoretical model of the frequency and temperature dependence of the complex dielectric constant of ferroelectric liquid crystals near the smectic-C* — smectic- A phase transition. Phys. Rev. A. 1990;42:877–889.

[22] Lagerwall ST. Ferroelectric and antiferroelectric liquid crystals. Newyork: WILEY-VCH; 1999.

[23] Mikułko A, Arora P, Glushchenko A, et al. Complementary studies of BaTiO 3 nanoparticles suspended in a ferroelectric liquid-crystalline mixture. Europhys. Lett. 2009;87:27009.

[24] Bartolino R, Doucet J, Durand G. Molecular tilt in the smectic C phase : a zigzag model. Ann. Phys. (Paris). 1978;3:389–395.

[25] Debnath A, Mandal PK. Dielectric properties of four room temperature ferroelectric and antiferroelectric multi- component liquid crystalline mixtures. Liq. Cryst. 2019;46:234–248.

[26] Debnath A, Mandal PK. Wide range room temperature ferroelectric liquid crystal mixture with microsecond order switching. J. Mol. Liq. 2016;221:287–291.

[27] Debnath A, Mandal PK, Węglowska D, et al. Induction of a room temperature ferroelectric SmC* phase in binary mixtures with moderate spontaneous polarization and sub-millisecond switching time. RSC Adv. 2016;6:84369–84378.

[28] Gorkunov M V., Giesselmann F, Lagerwall JPF, et al. Molecular model for de Vries type smectic A - smectic C phase transition in liquid crystals. Phys. Rev. E. 2007;75:060701.

[29] Kumar S. High-resolution x-ray measurements ofthe smectic phases ofterephthal-bis-(4n)-alkylanilines. Phys. Rev. A. 1981;23:3207–3214.

[30] Lagerwall JPF, Giesselmann F. Current Topics in Smectic Liquid Crystal Research. ChemPhysChem. 2006;7:20–45.

[31] Radcliffe MD, Brostrom ML, Epstein KA, et al. Smectic A and C materials with novel director tilt and layer thickness behaviour. Liq. Cryst. 1999;26:789–794.

[32] Roberts JC, Kapemaum N, Giesselmann F, et al. Design of liquid crystals with “de Vries-like” properties: Organosiloxane mesogen with a 5-phenylpyrimidine core. J. Am. Chem. Soc. 2008;130:13842–13843.

[33] Roberts JC, Song Q, Ayub K, et al. Design of liquid crystals with “de Vries-like” properties: Frustration between SmA- and SmC-promoting elements. J. Am. Chem. Soc. 2010;132:364–370.

[34] Kitzerow H, Bahr C, editors. Chirality in Liquid Crystals. New York: Springer; 2001.

[35] Manna U, Song J-K, Vij JK, et al. Anomalous dependence of response time on the electric field in an electroclinic liquid crystal with large induced tilt and polarization. Appl. Phys. Lett. 2009;94:012901.

[36] Bahr C, Heppke G. Infiuence of electric field on a first-order smectic-A —ferroelectric-smectic-C liquid-crystal phase transition: A field-induced critical point. Phys. Rev. A. 1990;41:4335–4342.

[37] Birgeneau RJ, Garland C, Kortan A, et al. Smectic-A —smectic-C transition: Mean field or critical. Phys. Rev. A. 1983;27:1251–1254.

[38] Prakash J, Chandran A, Biradar AM. Scientific developments of liquid crystal-based optical memory: a review. Reports Prog. Phys. 2017;80:016601.

[39] Naciri J, Ruth J, Crawford G, et al. Novel Ferroelectric and Electroclinic Organosiloxane Liquid Crystals. Chem. Mater. 1995;7:1397–1402.